Nature-Inspired DNA Nanosensor for Real-Time *in Situ* Detection of mRNA in Living Cells

Chor Yong Tay, Liang Yuan, and David Tai Leong*

Department of Chemical and Biomolecular Engineering, National University of Singapore, 4 Engineering Drive 4, 117585 Singapore, Singapore

ABSTRACT Rapid and precise *in situ* detection of gene expressions within a single cell is highly informative and offers valuable insights into its state. Detecting mRNA within single cells in real time and nondestructively remains an important challenge. Using DNA nanotechnology and inspired by nature's many examples of "protective-yet-accessible" exoskeletons, we designed our mRNA nanosensor, nano-snail-inspired nucleic acid locator (nano-SNEL), to illustrate these elements. The design of the nano-SNEL is composed of a sensory molecular beacon module to detect mRNA and a DNA nanoshell component, mimicking the functional anatomy of a snail. Accurate and sensitive visualization of mRNA is achieved by the exceptional protection conferred by the nanoshell to the sensory component from nucleases-mediated degradation by approximately 9−25-fold compared to its unprotected counterpart. Our nano-SNEL design strategy improved cell internalization is a demonstration of accurate, dynamic spatiotemporal resolved detection of RNA transcripts in living cells.

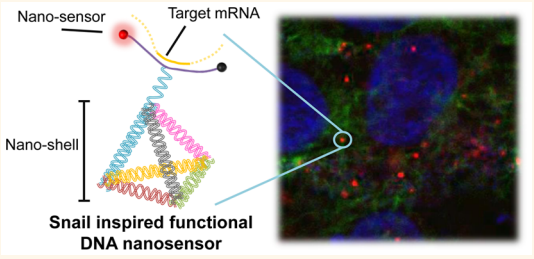

KEYWORDS: DNA nanostructures · biomimicry · nanotechnology · RNA detection · live cell imaging

Detection of intracellular elementary biomolecules such as proteins and nucleic acids in living cells, forms the foundational tenets of advancing our understanding in many aspects of cell biology, disease pathophysiology, drug discovery, medical diagnostics, and therapeutic applications.[1−3] Key to the successful and effective monitoring of single-cell dynamics is the development of quantitative and ultrasensitive imaging based detection of related biomarkers with specific recognition of targets in living cells. It is known that the cell fate, function, and phenotype are significantly dictated through the spatiotemporal control of messenger ribonucleic acid (mRNA) expression. Presently, several techniques for detecting mRNAs are available, which include *in situ* hybridization[4,5] and polymerase chain reaction (PCR).[6,7] However, these single-point and end-point techniques require the killing of the cells and are thus unable to capture the expression of mRNA in real time and real locality and high precision. More importantly, there is a seismic shift from total population gene expression measurements toward single-cell profiling. For example, this single-cell profiling is important in cancer, as the cancer tissue is complex and heterogeneous, consisting of cells of diverse genetic makeup. Working with the entire cancer tissue could provide only a population average of RNA expression and totally misses the important gene expression differences that occur in small subpopulations of cells or even single cells. The diversity thus gets drowned out in the sea of averaged noise. Even the cell-destructive RNA sequencing platform applied to single cells further supports our point of the need to investigate at the single-cell level. Genetically identical cells under the same situation may also exhibit diversified phenotypes due to the inherent stochasticity in gene expression.[8,9] To address these challenges, there has been growing interest in the development of optical probes for imaging RNA expression in live cells with high spatiotemporal resolution and at the single-cell level.

The use of molecular beacons (MBs) as an RNA sensor in a purified RNA environment, devoid of any other components except for nucleic acids, offers several advantages such as the possibility of detecting targets without the need to separate the bound and an excess of unbound probes and their relatively high signal-to-background ratio.[10−12]

* Address correspondence to cheltwd@nus.edu.sg.

Received for review April 1, 2015 and accepted April 23, 2015.

Published online April 23, 2015
10.1021/acsnano.5b01954

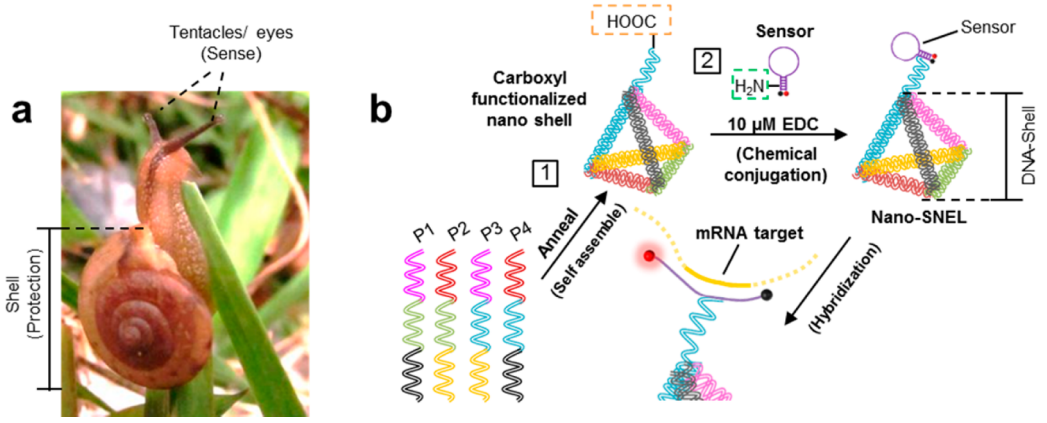

Figure 1. Design and working principle of nano-SNEL. (a) Image of the Asian tramp snail (*Bradybaena similaris*) that shows the typical anatomy of the gastropoda species, comprising a shell that is meant to provide essential protection from the harsh environment and whose movement is guided by the sensory organs. (b) Two-step synthesis scheme employed to construct nano-SNEL. The nanosensor (MB) is chemically conjugated to a pyramidal-shaped nanoshell that was designed to facilitate cellular entry and protect the sensor from nondiscriminatory digestion, which could lead to false negatives.

Obviously, a purified RNA environment would destroy the cell whose gene expression is what the MB is trying to probe. However, when applied for real-time detection of mRNA in intracellular environments, their usage is still hindered by some limitations including (a) the inability to pass through the cell membrane effectively and (b) nonspecific degradation of MB by intracellular enzymes such as DNase, which can lead to false positive signals.[13,14] To circumvent these drawbacks, the probe should therefore be protected from any potential unintended chemical change in the cytosol and yet be accessible to the mRNA of interest. Conventional approaches to protect the sensor with a physical barrier though conceptually sound may hinder the target molecules from reaching the sensor, leading to low signal gain and a drastic decrease in its sensing efficacy. So we reasoned that if we could strike the right balance between protecting the sensor and allowing it to bind freely to the RNA of interest and to facilitate its entry into the cell in the first place for any real-time and nondestructive detection of mRNA to occur, we might solve this important problem of detecting mRNA in the cell without destroying the cell.

The recent emergence of several bioinspired systems to sense biological molecules prompted us to turn to nature for inspiration.[15−18] Fortunately, nature has provided numerous simple yet elegant engineering solutions to this paradox as observed in numerous organisms such as the snail, which utilizes a "protective-yet-accessible" concept. For instance, snails' shells protect them from the harsh environment. When threatened, the soft body of the snail retracts into the protective shell. By integrating this biological system design concept using DNA nanotechnology,[19−22] we show that it is possible to construct a complex yet predictable DNA nanodevice to visualize targeted RNA in living cells.

In this study, inspired by the structural composition of the snail (Figure 1a), we designed a DNA-based mRNA nanosensor, termed nano-snail-inspired nucleic acid locator (nano-SNEL). Nano-SNEL was formed by conjugating a glyceraldehyde 3-phosphate dehydrogenase (GAPDH)-specific MB with a DNA-based nanoshell to provide both *in silico* and *in vitro* semiquantification measurement of GAPDH mRNA transcripts in living cells. We showed that nano-SNEL could synergistically present itself as an excellent intracellular probe, without interfering with either specific targeting by or hybridization-induced fluorescence of the beacon probes. Using human colorectal cell lines as *in vitro* models, nano-SNEL was shown to be noncytotoxic, display an innate ability to transfect the cells, and highly stable against nonspecific enzymatic degradation, which further decreases the likelihood of generating false positive signals. Consequently, when the cells were treated with nano-SNEL, robust *in situ* hybridized MB signals were attained and the associated intracellular spatial distribution could be mapped. The devised bioinspired nano-SNEL hybrid functional nanostructure is a highly stable and effective platform for the rapid detection of mRNA expression in living cells with a high level of specificity and at nanomolar sensitivity.

RESULTS AND DISCUSSION

Design of Snail-Inspired DNA-Based mRNA Sensor. Nano-SNEL is made up of two main components: (i) nanosensor and (ii) nanoshell (Figure 1b). The MB sensory apparatus is based on a fluorophore−quencher pair held close together by a complementary neck of a DNA hairpin. When hybridized with the complementary RNA target, the fluorophore separates from the quencher to generate an intense fluorescence signal. However, without protection, the sensor could generate false positive signals due to nonspecific degradation and interactions. To protect the DNA sensor, we hypothesized that attaching an additional DNA nanoshell[23−26] to the sensor could shield the sensor

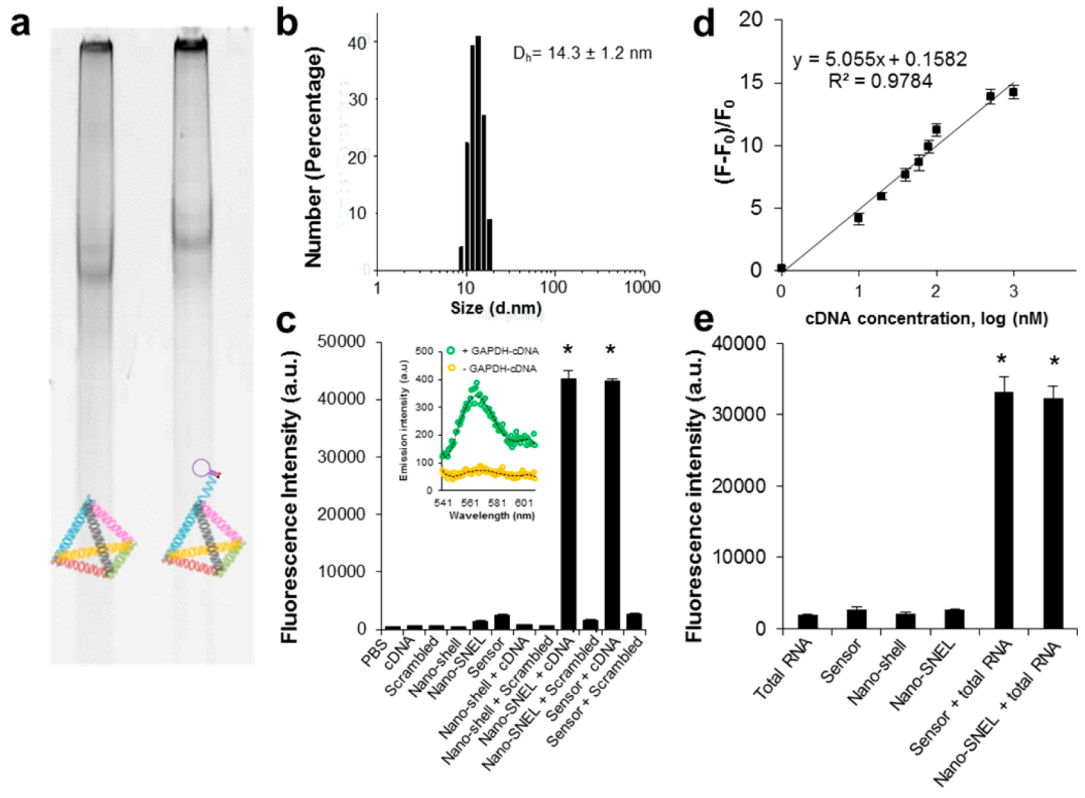

Figure 2. Characterization and *in silico* performance of nano-SNEL. (a) PAGE analysis showed reduced electrophoretic mobility of the nano-SNEL compared to the empty nanoshell counterpart. (b) DLS measurement revealed that the nano-SNEL has a mean hydrodynamic diameter of approximately 14 nm. (c) Complementary gene target specificity of nano-SNEL was validated by measuring the fluorescence enhancement upon hybridizing with the GAPDH-cDNA and scrambled form of the complementary target. Background fluorescence was established with a phosphate-buffered saline (PBS) solution. (d) The relative fluorescence intensity, $\Delta F = (F - F_0)/F_0$, measures the fold change in fluorescence intensity after hybridization with GAPDH-cDNA has occurred. F and F_0 were the fluorescence signals produced by the nanosensor measured with and without the complementary target. A linear relationship between ΔF and GAPDH-cDNA concentration (log scale) from 1 to 500 nM was observed. (e) *In silico* RNA detection of GAPDH transcript was also demonstrated with human SW480 colon adenocarcinoma derived total RNA samples. All data represent mean ± standard deviation from three replicates. * denotes statistical significance compared to the samples without the addition of complementary target. *$p < 0.05$.

from degradation, just like how the shell protects the snail body. Unlike other conventional nanocarriers, the nanoshell is unique because it is an "open" architecture, whereby the bioactive agents are exposed to a certain degree to target mRNA, yet being protected by virtue of its unique 3D nanoarchitecture against enzymatic breakdown.[27,28] Furthermore, these DNA nanostructures have high cell-uptake efficiencies.[29,30] The nanoshell was self-assembled from single-stranded DNA oligomers (P1−P4), averaging 55−65 base pairs (bp) each (see Supporting Information, Table S1).

Characterization and Validation of Nano-SNEL to Detect GAPDH mRNA Transcripts. Successful formation of the nanoshell was validated by use of polyacrylamide gel electrophoresis (PAGE) (see Supporting Information, Figure S1). Conjugation of the sensor to the DNA nanoshell was reflected with an almost 2-fold increase in the proportion of N−C(=O)−C species using X-ray photoelectron spectroscopy (Figure S2) due to the formation of amide bonds. Moreover, we observed a significant reduction in the electrophoretic mobility of the nano-SNEL compared to the DNA nanoshell alone (Figure 2a), which could be attributed to the increased molecular mass and more complex spatial structure of the nano-SNEL. Dynamic light scattering (DLS) measurement revealed nano-SNEL has a mean hydrodynamic diameter of approximately 14 nm (Figure 2b).

GAPDH mRNA was chosen as our target due to its ubiquity and biological significance.[31] As shown in the Figure 2c inset, a fluorescence maximum at 564 nm could be detected when the 19 bp synthetic GAPDH-cDNA hybridized with the MB component of the nano-SNEL. Furthermore, there is a lack of significant fluorescence increment when the probes were incubated with the scrambled form of GAPDH-cDNA, suggesting that nano-SNEL is highly specific in recognizing the intended target (Figure 2c). We also showed that the MB sensor was stably attached to the DNA nanoshell (Figure S3). We observed a gradual linear increase in ΔF with increasing cDNA concentrations from 1 nM to 500 nM (Figure 2d). The detection limit was 0.94 nM for *in silico* GAPDH-cDNA sensing. Next, we used nano-SNEL to measure total RNA samples isolated from SW480 cells (Figure 2e). Negligible fluorescence signal

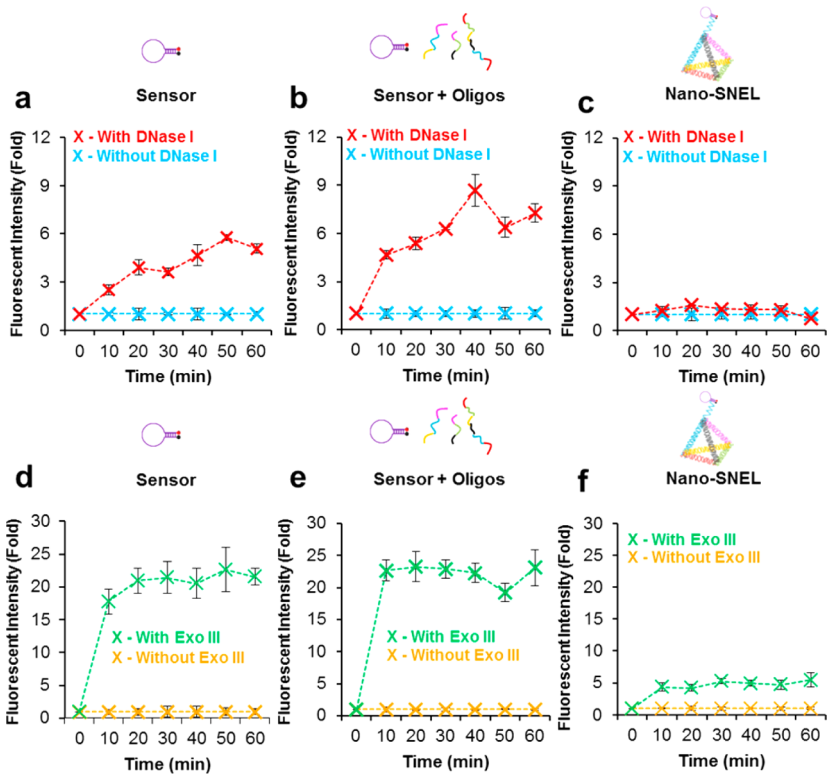

Figure 3. Nano-SNEL exhibits protective effects to the MB against nuclease-mediated degradation. Nonspecific degradation of the MB sensor may lead to the generation of no specific Cy3 fluorescence signal, even in the absence of complementary target. Fluorescence−time graph depicting probe opening of the sensor due to (a−c) human DNase I and (d−f) Exo III induced degradation.

was detected in the total RNA, sensor, and nano-SNEL groups without the complementary target. Conversely, the nano-SNEL and sensor samples generated a significant increase in fluorescence signal when incubated with the total RNA samples, suggesting that nano-SNEL could detect mRNA target without any reverse transcription reaction, an important point in any real-time in-cell mRNA detection application.

Nano-SNEL Displays Excellent Enzymatic Resistance. It is important to protect the sensor from both extracellular and intracellular degradation during the perilous passage to the vicinity of target mRNA, as degradation would produce false positives.[32,33] To examine the ability of nano-SNEL to resist nuclease attack, the samples were treated with 3U/mL of human deoxyribonuclease (DNase) I and exonuclease III (Exo III). DNase I is a potent endonuclease capable of degrading both single- and double-stranded DNA completely to yield 5′-phosphate-terminated polynucleotides,[34] whereas Exo III facilitates progressive removal of nucleotides from the 3′-hydroxyl-terminated ends of duplex DNA.[35] Any digestion of the sensor could be detected as spontaneous fluorescence, due to the physical separation of the fluorophore (Cy3) from the quencher. Figure 3a−f shows the fluorescence−time curves that are representative of the degradation process. DNase I treatment caused the "naked" sensor to degrade, as exemplified by a gradual increase in Cy3 signal with increasing incubation time (Figure 3a). The fluorescence signal plateaus at around 40 min, corresponding to an approximately 6-fold increase. The same but unassembled oligomers used to construct the nanoshell offered little protection from the nucleases (Figure 3b), indicative that increasing DNA content alone did not confer any form of protection to the sensor. In contrast, DNase I treatment did not lead to any significant fluorescence enhancement in the nano-SNEL sample (Figure 3c), suggesting that the conjugated nanoshell is capable of protecting the sensor from the nuclease. When the samples were treated with Exo III, we again observed that the unprotected sensor was susceptible to nuclease attack (Figure 3d,e). Yet, in the nano-SNEL configuration, there is a substantial improvement in terms of shielding the sensor from the digestive effects of the Exo III enzyme throughout the 1 h treatment time (Figure 3f).

Probing deeper into the protective mechanism, we monitored the structural integrity of the nano-SNEL using PAGE. Samples were treated with either DNase I or Exo III at 37 °C and collected at predetermined time points. With increasing incubation time with DNase I, a gradual smearing of the bands could be detected, indicative that the nano-SNEL component was being degraded (Figure 4a). This suggests that the nanoshell is playing a sacrificial role that shields the sensor from the effects of DNase I. Compared to the unprotected sensor, there is a substantial delay before any apparent

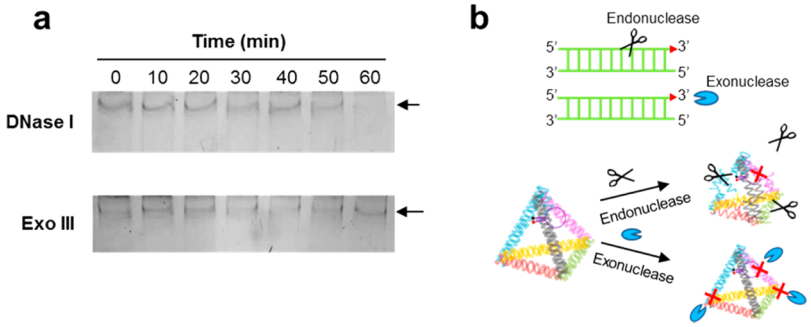

Figure 4. Distinctive protective mechanism against endo and exo nuclease by nano-SNEL. (a) PAGE gel analysis of nuclease-treated samples to examine the structural integrity of nano-SNEL. (b) Schematics to illustrate how endonuclease and exonuclease cleave the phosphodiester bonds and the proposed protective mechanism conferred to the sensor by the nano-SNEL. Our results suggest that the DNA shell can function like a nanoarmament to the sensor and/or provide steric hindrance, protecting it from digestion and thus reduce the likelihood of generating false positive signals.

degradation of nano-SNEL that could be detected. This phenomenon could be attributed to the enzymatic resistant property that is intrinsic to the DNA nanoshell,[27,36] making DNA-based 3D complex nanostructures extremely useful as vehicles. Conversely, Exo III treatment has minimal degradation effects on the nano-SNEL (Figure 4a, lower panel). Unlike DNase I, which could bind randomly to the DNA, Exo III exhibits site-specific binding at the 3′ end to cleave the phosphodiester bond of DNA (Figure 4b). We reasoned that the nanoshell was designed to adopt a "closed loop" configuration, thus avoiding any free-hanging 3′ termini. As shown in Figure 3f, the presence of the nanoshell, although reduced, could not entirely inhibit Exo III-mediated digestion of the sensor, suggesting that a more subtle protective mechanism might be at play. Since the sensor was anchored at the vertex of the nanoshell (Figure 1b), its actual relative position is in close proximity to the DNA nanoshell or even inside the void of the shell, making it difficult for the nucleases to access the MB sensor sufficiently to degrade it. Such steric impediment is possible since the exact position of the sensor is not spatially fixed. Conceptually, the sensor is covalently tethered to the shell, separated by a thymine-based nucleotide arm that is 10 bp long. This is more than half the length (17 bp) of the pyramidal strut, and thus the sensor can move with certain degrees of freedom with the nanoshell vertex as a pivot point. Collectively, we show that the nanoshell could impart nuclease resistance to the sensor, reminiscent of how the shell protects the vulnerable snail from harsh environmental threats. (Figure 4b).

***In Vitro* Cellular Uptake and Biodistribution of DNA Nanostructure.** In order for the proposed nano-SNEL to be effective as an intracellular mRNA sensor, there is a need to determine the biocompatibility and subcellular distribution upon gaining entry into the cells. Internalization of nanoscale materials is a highly complex process that is influenced by a plethora of factors including particle size, surface chemistries, and cell types.[37−43] Understanding the intracellular fate and mechanisms of nano-SNEL will aid in rational future design for more advanced applications. Using DLD-1 and SW480 human colon adenocarcinoma cells, we observed that nano-SNEL was essentially noncytotoxic and highly biocompatible for at least 24 h (Figure S4). Next, the Cy3-tagged nanoshell was used as a surrogate to determine the uptake and intracellular distribution of the nano-SNEL. As shown in Figure 5a, cellular uptake of the DNA nanostructure was drastically reduced at 4 °C as compared to 37 °C, regardless of the cell type. This suggests that nano-SNEL uptake is most likely to proceed *via* an energy-dependent process. Once internalized, nano-SNEL might be transported and degraded in the lysosomes, thus missing the intended target RNA.[14] The fluorescent nanoshell was found to be distributed within the cytoplasm but not in the nucleus. Low PCC and M1 and M2 (all <0.15) values suggest that the majority of the internalized nanoshell did not reside within the lysosomes (Figure 5b), making them suitable as an intracellular mRNA sensor.

Application of Nano-SNEL to Image GAPDH mRNA Expression in Living Cells. Next, we examined the capability of the nano-SNEL to detect GAPDH mRNA expression in both DLD-1 and SW480 cells. Within 1 h of incubation with 2.5 nM nano-SNEL, fluorescence signals (GAPDH-hybridized nano-SNEL) were readily visible in both cell types (Figure 6c and f). Conversely, cells treated with the "naked" sensor (Figure 6b and e) did not express any red fluorescent signals. This could be attributed to the sensor's inherent inability to penetrate into the cells. Attachment of the nanoshell to the sensor greatly enhanced cellular internalization. Furthermore, in agreement with our colocalization studies, we noted that there was no overlapping of hybridized nano-SNEL signal with lysosomes. Previous studies have tried numerous methods such as reversible cell membrane permeabilization,[44] microinjection,[45] and electroporation[32] to deliver DNA materials into the cells for real-time detection of the mRNA target in living cells. The invasive nature of such approaches also limited their applications *in vivo*.

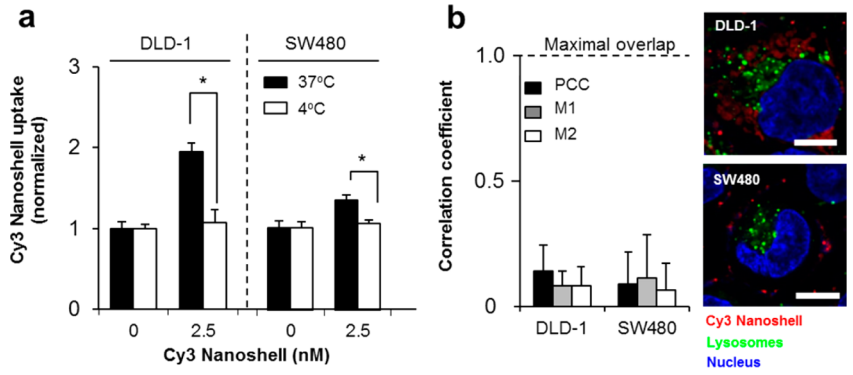

Figure 5. Nanoshell cellular uptake and subcellular distribution. (a) Uptake of Cy3-conjugated nanoshell was significantly decreased when the temperature was dropped to 4 °C in both DLD-1 and SW480 cells. (b) Colocalization analysis of the nanoshell and lysosome was conducted based on the high-resolution confocal microscopy images. Cell nuclei and lysosomes were counterstained with Hoechst dye (blue) and LysoTracker Green, respectively (green). Maximal overlap of both red and green channels is denoted by a correlation value of 1. A low numerical value of the Pearson's correlation coefficient (PCC) and overlapping coefficients (M1 and M2) suggest that there is minimal nanoshell residing within the acidic lysosomes. All data represent mean ± standard deviation from three replicates. * denotes statistical significance. *$p < 0.05$. Scale bar = 10 μm.

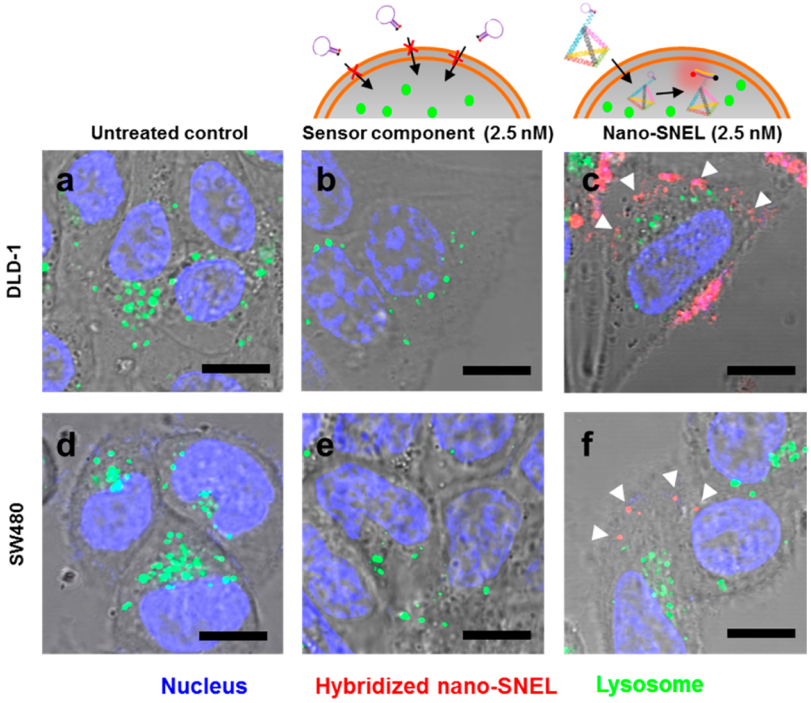

Figure 6. *In vitro* spatiotemporal mapping of GAPDH mRNA transcript in human colorectal adenocarcinoma cell lines. Composite fluorescence and bright-field images of DLD-1 and SW480 cells costained for cell nucleus (blue) and acidic lysosomal compartments (green). Untreated samples serve as negative control (a and d). Cells were treated with either 2.5 nM MB alone (b and e) or nano-SNEL (c and f). Detection of cytoplasmic GAPDH mRNA complementary target in both cell types (red) could be observed only in the nano-SNEL-treated groups, while the MB-treated group did not show any detection. In both MB and nano-SNEL treatment groups, there is no coaddition of any transfection reagent. Scale bar = 10 μm.

In contrast, our proposed platform offers unprecedented delivery of the mRNA sensor into the cells in a noninvasive manner. Our results are consistent with previous studies that showed complex DNA-based nanostructures possess the innate ability to cross the cell membrane and have been exploited to deliver therapeutic agents such as doxorubicin,[46] cytosine-phosphate-guanosine (CpG) oligonucleotide,[36] actinomycin D,[24] and siRNA.[30]

CONCLUSION

In summary, our results demonstrated the potential of the devised snail-inspired nanosensor to detect and map the spatiotemporal distribution of mRNA transcript in living cells. The concept of the nano-SNEL exploited the natural synergy between the nanosensor and nanoshell motifs to facilitate delivery of the nano-SNEL into the cells, without the misleading issues of

false positive signals due to enhanced resistance to enzymatic degradation and avoiding the lysosomal pathway. The four vertices of the DNA nanoshell are simple but profoundly useful, as they can also allow multiplexing of up to four different RNA sensors on the same unit. This first generation of DNA nanosensors based on the concept of protective-yet-accessible for biosensing applications can be further improved to have increased stability through using optical isomers of nucleotides.[47] By incorporating stimuli-responsive switches,[21,48] one can give several levels of responsiveness and sophistication for more intricate bioapplications in cancer, metabolic diseases, and stem cell areas. Conceptually, we can now monitor any RNA species, including viral RNA (*e.g.*, Ebola, HIV, and dengue), without any extensive processing steps (as compared to classical qPCR), which could prove to be very important in an epidemic situation.

METHODS

Preparation of the Nano-SNEL. A two-step synthesis approach was employed to synthesize the nano-SNEL. The first step entails the formation of the DNA nanopyramidal shell. The nanoshell was self-assembled according to previous reports.[23−25] Four customized oligonucleotide strands (P1, P2, P3, and P4) were diluted with TE buffer (10 mM Tris, 1 mM EDTA, pH 8.0) to a common final concentration of 10 μM. The four oligonucleotide solutions were then mixed in equimolar quantities in TM buffer (20 mM Tris, 50 mM $MgCl_2$, pH 8.0), heated to 95 °C for 2 min using an MJ Mini Personal Thermal Cycler (Bio-Rad Laboratories Ltd., Singapore), and then immediately cooled on ice for at least 1 min. Next, to the as-synthesized nanoshell, the GAPDH molecular beacon nanosensor was conjugated to the carboxyl-functionalized P1 oligonucleotide at the 5′ terminus. The third base from the 3′ end on the quencher arm of the sensor was functionalized with a modified nucleotide dT-amine group linked through a six-carbon spacer. Conjugation reaction of the DNA nanoshell and GAPDH nanosensor was carried out for 2 h at room temperature under continuous shaking in a tube with a final volume of 400 μL containing equimolar concentrations of the nanoshell and sensor (50 nM), 2 μM 1-ethyl-3-[3-(dimethylamino)propyl]carbodiimide hydrochloride (EDC) (freshly prepared), and 1× PBS (pH 7.4). The obtained nano-SNEL complex was purified by centrifugation at 12000*g* for 5 min by using Thermo Scientific Pierce concentrators (MWCO-30K, 0.5 mL). The nano-SNEL conjugate in this manner was dispersed in 1× PBS (pH 7.4) and stored at 4 °C with a final concentration of 200 nM.

Characterization of the Nano-SNEL. The nanoshell and nano-SNEL were characterized using PAGE, DLS, and X-ray photoelectron spectroscopy (XPS). PAGE gel analysis for the nanoshell and nano-SNEL was conducted using a 12.5% or 10% nondenaturing polyacrylamide gel in ice-cold 1× TBE (tris borate-EDTA) buffer, respectively. The gels were run at a constant voltage of 120 V for 2 h. DLS was employed to measure the hydrodynamic size of the nano-SNEL. Briefly, 50 μL of nano-SNEL solution (200 nM) was first centrifuged at high speed at 13000*g* for an hour at 4 °C, before the supernatant (35 μL) was retrieved and the hydrodynamic diameter in ultrapure water was determined using the Zetasizer Nano ZS (Malvern). For the XPS analysis, the nano-SNEL (200 nM) samples were dropped onto a glass slide and air-dried overnight, before the samples were analyzed with the XPS (AXIS HIS, Kratos Analytical), equipped with a mono Al Kα radiation source ($h\nu$ = 1486.71 eV). The analysis was conducted with the following operating parameters: 15 kV and 5 mA. The raw XPS signal was then processed and deconvoluted with the XPSPEAK 4.1 software using the C 1s peak (284.5 eV) as an internal control.

Detection of Complementary GAPDH Targets with Nano-SNEL. The ability for the nano-SNEL to detect GAPDH mRNA targets was determined using the Synergy H1 hybrid multimode microplate reader (Bio-Tek). Cy3 fluorescence signal was determined with an excitation and emission wavelength of 512 and 564 nm. The concentration of the pristine sensor or nano-SNEL used for the fluorescence studies was 10 nM in 1× PBS (pH 7.4), and probe−target hybridization was detected in an excess amount of synthetic complementary GAPDH strands (Table S1) or total RNA that was isolated from SW480 cell lines, using the RNeasy mini kit (Qiagen). The fluorescence signal of the hybridized sensor was recorded as the background signal.

Nuclease-Mediated Degradation of the Nano-SNEL. Digestion of the GAPDH-sensor was probed using the Synergy H1 hybrid multimode microplate reader (Bio-Tek) to detect generation of nonspecific Cy3 fluorescent signals. For both human DNase I (Thermo Scientific) and exonuclease III (New England Biolabs) digestion, a common concentration of 3U/mL was used to digest 10 nM DNA samples in PBS. Cy3 signal was monitored and recorded over a period of 1 h at 10 min intervals at 37 °C. Solutions of digested mixtures were analyzed with PAGE using 12.5% gel, run at 150 V for 1 h in ice-cold 1× TBE buffer.

Cell Viability Assay. DLD-1 and SW480 human colorectal adenocarcinoma cells (ATCC) were cultured at an initial seeding density of 50 000 cells/cm^2 in 24-well plates overnight in Dulbecco's modified Eagle's media (DMEM; Gibco) supplemented with 10% fetal bovine serum (FBS, Thermo Scientific) and 1% penicillin and streptomycin solution (PAA Laboratories Inc.) respectively. Thereafter, the cells were treated with varying concentrations of nano-SNEL for 24 h and the cells were harvested using trypsin. To differentiate the viable and nonviable cells, the cells were stained with TALI Viability kit-Dead Cell Green that is normally impermeable to viable cells but able to stain the nucleus of dead cells green. Percentage of viable cells was analyzed using the TALI image cytometer.

Cellular Uptake and Subcellular Distribution of Nano-SNEL. DLD-1 and SW480 cells were cultured overnight at an initial seeding density of 50,000 cells/cm^2 in Dulbecco's Modified Eagle's Media (DMEM; Gibco) supplemented with 10% FBS (Thermo Scientific) and 1% penicillin and streptomycin solution (PAA Laboratories Inc., USA), and cells were cultured under standard culture conditions. Following this, the cell nucleus were labeled with Hoechst 33342 fluorescent DNA dye (1 μg/mL) at 37 °C for 30 min, before the cells were treated with fluorescently labeled DNA nanostructures, prepared using the Cy3-conjugated oligonucleotide strand P1 during the formation of the nanoshell. Cells were incubated with the fluorescent DNA nanostructure for 2 h at either 4 or 37 °C. Samples were subsequently retrieved and washed three times with PBS, and the fluorescence signals were measured with the Cytation 3 multimode plate reader (BioTek) with em 512/ex 564 and em 350/ex 420 to detect the presence of the nano-SNEL and cell nucleus, respectively. The fluorescence signal produced by the internalized nanosensor was normalized to the number of cells (as indicated by the Hoechst 33342 DNA dye signal) to reflect the overall uptake of the nano-SNEL. To examine the subcellular localization of the nano-SNEL, the cells were prelabeled with LysoTracker Green DND-26 (Molecular Probes) for 30 min at a concentration of 75 nM at 37 °C, before incubating with the DNA samples for a further 1 h. To visualize the Cy3-conjugated nanoshell or hybridized nano-SNEL and lysosomes, high-resolution confocal microscopic images were captured using a 60× oil immersion objective lens on the Olympus FV100 confocal microscope and processed using the Olympus Fluoview software. All images were taken the same day using the same exposure and gain. Computation of the colocalization parameters was done on the ImageJ platform *via* the "Just Another Colocalization" Plugin (JACoP). Seventeen randomly selected cells were chosen to

examine the degree of overlapping signals that were derived from the lysosome and Cy3-conjugated nanoshell.

Statistical Analysis. All experiments were conducted in triplicate. Data are mean ± standard deviation. Statistical analysis was performed using Original 9 (OriginLab). Experimental data were subjected to Student's *t* test where applicable, and statistical significance was ascertained at a confidence level of $p < 0.05$.

Conflict of Interest: The authors declare no competing financial interest.

Supporting Information Available: Additional experimental data in Table S1 and Figures S1–S4 are available free of charge on the ACS Publications website at DOI: 10.1021/acsnano.5b01954.

Acknowledgment. This work was supported by a NUS Engineering-Medicine Cross-Faculty grant (R279000414112) to D.T.L. C.Y.T. gratefully acknowledges support from the Lee Kuan Yew Postdoctoral Fellowship. C.Y.T, L.Y., and D.T.L. conceived the design of nanosensors and the experiments. C.Y.T. and Y.L. performed the experiments. C.Y.T. and D.T.L. analyzed the data and made the conclusions. C.Y.T. and D.T.L. wrote the manuscript.

REFERENCES AND NOTES

1. Spiller, D. G.; Wood, C. D.; Rand, D. A.; White, M. R. H. Measurement of Single-Cell Dynamics. *Nature* **2010**, *465*, 736–745.
2. Chattopadhyay, P. K.; Gierahn, T. M.; Roederer, M.; Love, J. C. Single-Cell Technologies for Monitoring Immune Systems. *Nat. Immunol.* **2014**, *15*, 128–135.
3. Wills, Q. F.; Livak, K. J.; Tipping, A. J.; Enver, T.; Goldson, A. J.; Sexton, D. W.; Holmes, C. Single-Cell Gene Expression Analysis Reveals Genetic Associations Masked in Whole-Tissue Experiments. *Nat. Biotechnol.* **2013**, *31*, 748–752.
4. Bassell, G. J.; Powers, C. M.; Taneja, K. L.; Singer, R. H. Single mRNAs Visualized by Ultrastructural *in Situ* Hybridization are Principally Localized at Actin Filament Intersections in Fibroblasts. *J. Cell Biol.* **1994**, *126*, 863–876.
5. Paik, J. H.; Choe, G.; Kim, H.; Choe, J. Y.; Lee, H. J.; Lee, C. T.; Lee, J. S.; Jheon, S.; Chung, J. H. Screening of Anaplastic Lymphoma Kinase Rearrangement by Immunohistochemistry in Non-Small Cell Lung Cancer Correlation with Fluorescence *in Situ* Hybridization. *J. Thorac. Oncol.* **2011**, *6*, 466–472.
6. Gong, C.; Maquat, L. E. lncRNAs Transactivate STAU1-Mediated mRNA Decay by Duplexing with 3′ UTRs *via* Alu Elements. *Nature* **2011**, *470*, 284–288.
7. Moore, M. J.; Wang, Q.; Kennedy, C. J.; Silver, P. A. An Alternative Splicing Network Links Cell-Cycle Control to Apoptosis. *Cell* **2010**, *142*, 625–636.
8. Elowitz, M. B.; Levine, A. J.; Siggia, E. D.; Swain, P. S. Stochastic Gene Expression in a Single Cell. *Science* **2002**, *297*, 1183–1186.
9. Mettetal, J. T.; Muzzey, D.; Pedraza, J. M.; Ozbudak, E. M.; van Oudenaarden, A. Predicting Stochastic Gene Expression Dynamics in Single Cells. *Proc. Natl. Acad. Sci. U.S.A.* **2006**, *103*, 7304–7309.
10. Wang, K.; Tang, Z.; Yang, C. J.; Kim, Y.; Fang, X.; Li, W.; Wu, Y.; Medley, C. D.; Cao, Z.; Li, J.; *et al*. Molecular Engineering of DNA: Molecular Beacons. *Angew. Chem., Int. Ed.* **2009**, *48*, 856–870.
11. Kim, E.; Yang, J.; Park, J.; Kim, S.; Kim, N. H.; Yook, J. I.; Suh, J.-S.; Haam, S.; Huh, Y.-M. Consecutive Targetable Smart Nanoprobe for Molecular Recognition of Cytoplasmic microRNA in Metastatic Breast Cancer. *ACS Nano* **2012**, *6*, 8525–8535.
12. Tyagi, S.; Bratu, D. P.; Kramer, F. R. Multicolor Molecular Beacons for Allele Discrimination. *Nat. Biotechnol.* **1998**, *16*, 49–53.
13. Kim, Y.; Sohn, D.; Tan, W. Molecular Beacons in Biomedical Detection and Clinical Diagnosis. *Int. J. Clin. Exp. Pathol.* **2008**, *1*, 105–116.
14. Chen, A. K.; Behlke, M. A.; Tsourkas, A. Avoiding False-Positive Signals with Nuclease-Vulnerable Molecular Beacons in Single Living Cells. *Nucleic Acids Res.* **2007**, *35*, e105.
15. Mao, C. B.; Liu, A.; Cao, B. Virus-Based Chemical and Biological Sensing. *Angew. Chem., Int. Ed.* **2009**, *48*, 6790–6810.
16. Liu, A.; Abbineni, G.; Mao, C. B. Nanocomposite Films Assembled from Genetically Engineered Filamentous Viruses and Gold Nanoparticles: Nanoarchitecture- and Humidity-Tunable Surface Plasmon Resonance Spectra. *Adv. Mater.* **2009**, *21*, 1001–1005.
17. Wang, M.; Hou, W.; Mi, C. C.; Wang, W. X.; Xu, Z. R.; Teng, H. H.; Mao, C. B.; Xu, S. K. Immunoassay of Goat Antihuman Immunoglobulin G Antibody Based on Luminescence Resonance Energy Transfer between Near-Infrared Responsive $NaYF_4$:Yb, Er Upconversion Fluorescent Nanoparticles and Gold Nanoparticles. *Anal. Chem.* **2009**, *81*, 8783–8789.
18. Wang, Y.; Ju, Z.; Cao, B.; Gao, X.; Zhu, Y.; Qiu, P.; Xu, H.; Pan, P.; Bao, H.; Wang, L.; *et al*. Ultrasensitive Rapid Detection of Human Serum Antibody Biomarkers by Biomarker-Capturing Viral Nanofibers. *ACS Nano* **2015**, 10.1021/acsnano.5b01074.
19. Perrault, S. D.; Shih, W. M. Virus-Inspired Membrane Encapsulation of DNA Nanostructures to Achieve *in Vivo* Stability. *ACS Nano* **2014**, *8*, 5132–5140.
20. Hahn, J.; Wickham, S. F. J.; Shih, W. M.; Perrault, S. D. Addressing the Instability of DNA Nanostructures in Tissue Culture. *ACS Nano* **2014**, *8*, 8765–8775.
21. Liu, Z.; Tian, C.; Yu, J.; Li, Y.; Jiang, W.; Mao, C. B. Self-Assembly of Responsive Multilayered DNA Nanocages. *J. Am. Chem. Soc.* **2015**, *137*, 1730–1733.
22. Deng, Z. X.; Lee, S. H.; Mao, C. D. DNA as Nanoscale Building Blocks. *J. Nanosci. Nanotechnol.* **2005**, *5*, 1954–1963.
23. Yuan, L.; Giovanni, M.; Xie, J.; Fan, C.; Leong, D. T. Ultrasensitive IgG Quantification using DNA Nano-Pyramids. *NPG Asia Mater.* **2014**, *6*, e112.
24. Setyawati, M. I.; Kutty, R. V.; Tay, C. Y.; Yuan, X.; Xie, J.; Leong, D. T. Novel Theranostic DNA Nanoscaffolds for the Simultaneous Detection and Killing of Escherichia coli and Staphylococcus aureus. *ACS Appl. Mater. Interfaces* **2014**, *6*, 21822–21831.
25. Giovanni, M.; Setyawati, M. I.; Tay, C. Y.; Hang, Q.; Kuan, W. S.; Leong, D. T. Electrochemical Quantification of Escherichia coli with DNA Nanostructure. *Adv. Funct. Mater.* **2015**, 10.1002/adfm.201500940.
26. Goodman, R. P.; Berry, R. M.; Turberfield, A. J. The Single-Step Synthesis of a DNA Tetrahedron. *Chem. Commun.* **2004**, 1372–1373.
27. Keum, J. W.; Bermudez, H. Enhanced Resistance of DNA Nanostructures to Enzymatic Digestion. *Chem. Commun.* **2009**, 7036–7038.
28. Mei, Q.; Wei, X.; Su, F.; Liu, Y.; Youngbull, C.; Johnson, R.; Lindsay, S.; Yan, H.; Meldrum, D. Stability of DNA Origami Nanoarrays in Cell Lysate. *Nano Lett.* **2011**, *11*, 1477–1482.
29. Walsh, A. S.; Yin, H.; Erben, C. M.; Wood, M. J. A.; Turberfield, A. J. DNA Cage Delivery to Mammalian Cells. *ACS Nano* **2011**, *5*, 5427–5432.
30. Lee, H.; Lytton-Jean, A. K. R.; Chen, Y.; Love, K. T.; Park, A. I.; Karagiannis, E. D.; Sehgal, A.; Querbes, W.; Zurenko, C. S.; Jayaraman, M.; Peng, C. G.; *et al*. Molecularly Self-Assembled Nucleic Acid Nanoparticles for Targeted *in Vivo* siRNA Delivery. *Nat. Nanotechnol.* **2012**, *7*, 389–393.
31. Sirover, M. A. Role of the Glycolytic Protein, Glyceraldehyde-3-Phosphate Dehydrogenase, in Normal Cell Function and in Cell Pathology. *J. Cell. Biochem.* **1997**, *66*, 133–140.
32. Chen, A. K.; Behlke, M. A.; Tsourkas, A. Efficient Cytosolic Delivery of Molecular Beacon Conjugates and Flow Cytometric Analysis of Target RNA. *Nucleic Acids Res.* **2008**, *36*, e69.
33. Luo, D.; Saltzman, W. M. Synthetic DNA Delivery Systems. *Nat. Biotechnol.* **2000**, *18*, 33–37.
34. Kishi, K.; Yasuda, T.; Takeshita, H. DNase I: Structure, Function, and Use in Medicine and Forensic Science. *Leg. Med. (Tokyo)* **2001**, *3*, 69–83.
35. Henikoff, S. Unidirectional Digestion with Exonuclease III Creates Targeted Breakpoints for DNA Sequencing. *Gene* **1984**, *28*, 351–359.
36. Li, J.; Pei, H.; Zhu, B.; Liang, L.; Wei, M.; He, Y.; Chen, N.; Li, D.; Huang, Q.; Fan, C. Self-Assembled Multivalent

DNA Nanostructures for Noninvasive Intracellular Delivery of Immunostimulatory CpG Oligonucleotides. *ACS Nano* **2011**, *5*, 8783–8789.
37. Tay, C. Y.; Yu, Y.; Setyawati, M. I.; Xie, J.; Parak, W. J.; Leong, D. T. Back to Basics: Exploiting the Innate Physico-chemical Characteristics of Nanomaterials for Biomedical Applications. *Adv. Funct. Mater.* **2014**, *24*, 5936–5955.
38. Tay, C. Y.; Yu, Y.; Setyawati, M. I.; Xie, J.; Leong, D. T. Presentation Matters: Identity of Gold Nanocluster Capping Agent Governs Intracellular Uptake and Cell Metabolism. *Nano Res.* **2014**, *7*, 805–815.
39. Gandra, N.; Wang, D. D.; Zhu, Y.; Mao, C. B. Virus-Mimetic Cytoplasm-Cleavable Magnetic/Silica Nanoclusters for Enhanced Gene Delivery to Mesenchymal Stem Cells. *Angew. Chem., Int. Ed.* **2013**, *52*, 11278–11281.
40. Shi, Z. Z.; Ren, W. Z.; Gong, A.; Zhao, X. M.; Zou, Y. H.; Brown, E. M. B.; Chen, X. Y.; Wu, A. G. Stability Enhanced Polyelectrolyte-Coated Gold Nanorod-Photosensitizer Complexes for High/Low Power Density Photodynamic Therapy. *Biomaterials* **2014**, *35*, 7058–7067.
41. Ma, K.; Wang, D.-D.; Lin, Y.; Wang, J.; Petrenko, V.; Mao, C. B. Synergetic Targeted Delivery of Sleeping-Beauty Transposon System to Mesenchymal Stem Cells Using LPD Nanoparticles Modified with a Phage-Displayed Targeting Peptide. *Adv. Funct. Mater.* **2013**, *23*, 1172–1181.
42. Cao, B.; Yang, M.; Zhu, Y.; Qu, X.; Mao, C. B. Stem Cells Loaded with Nanoparticles as a Drug Carrier for *in Vivo* Breast Cancer Therapy. *Adv. Mater.* **2014**, *26*, 4627–4631.
43. Cao, B.; Qiu, P.; Mao, C. B. Mesoporous Iron Oxide Nanoparticles Prepared by Polyacrylic Acid Etching and their Application in Gene Delivery to Mesenchymal Stem Cells. *Microsc. Res. Technol.* **2013**, *76*, 936–941.
44. Santangelo, P. J.; Nix, B.; Tsourkas, A.; Bao, G. Dual FRET Molecular Beacons for mRNA Detection in Living Cells. *Nucleic Acids Res.* **2004**, *32*, e57.
45. Medley, C. D.; Drake, T. J.; Tomasini, J. M.; Rogers, R. J.; Tan, W. Simultaneous Monitoring of the Expression of Multiple Genes Inside of Single Breast Carcinoma Cells. *Anal. Chem.* **2005**, *77*, 4713–4718.
46. Kim, K. R.; Kim, D. R.; Lee, T.; Yhee, J. Y.; Kim, B. S.; Kwon, I. C.; Ahn, D. R. Drug Delivery by a Self-Assembled DNA Tetrahedron for Overcoming Drug Resistance in Breast Cancer Cells. *Chem. Commun.* **2013**, *49*, 2010–2012.
47. Kim, K.-R.; Lee, T.; Kim, B.-S.; Ahn, D.-R. Utilizing the Bioorthogonal Base-Pairing System of I-DNA to Design Ideal DNA Nanocarriers for Enhanced Delivery of Nucleic Acid Cargos. *Chem. Sci.* **2014**, *5*, 1533–1537.
48. Modi, S.; Swetha, M. G.; Goswami, D.; Gupta, G. D.; Mayor, S.; Krishnan, Y. A DNA Nanomachine That Maps Spatial and Temporal pH Changes inside Living Cells. *Nat. Nanotechnol.* **2009**, *4*, 325–330.